

A combined airfoil with secondary feather inspired by the golden eagle and its influences on the aerodynamics

Di Tang(唐迪), Zhongyong Fan(范忠勇), Mingxia Lei(雷鸣霞), Binbin Lv(吕彬彬), Li Yu(余立), Hao Cui(崔浩)

Citation: Chin. Phys. B . 2019, 28(3): 034702. **doi:** 10.1088/1674-1056/28/3/034702
Journal homepage: http://cpb.iphy.ac.cn; http://iopscience.iop.org/cpb

What follows is a list of articles you may be interested in

Aerodynamic measurement of a large aircraft modelin hypersonic flow

Bao-Qing Meng(孟宝清), Gui-Lai Han(韩桂来), De-Liang Zhang(张德良), Zong-Lin Jiang(姜宗林)

Chin. Phys. B . 2017, 26(11): 114702. **doi:** 10.1088/1674-1056/26/11/114702

Experimental investigation on underwater drag reduction using partial cavitation

Bao Wang(王宝), Jiadao Wang(汪家道), Darong Chen(陈大融), Na Sun(孙娜), Tao Wang(王涛)

Chin. Phys. B . 2017, 26(5): 054701. **doi:** 10.1088/1674-1056/26/5/054701

Experimental investigations of detonation initiation by hot jets in supersonic premixed flows

Han Xu, Zhou Jin, Lin Zhi-Yong

Chin. Phys. B . 2012, 21(12): 124702. **doi:** 10.1088/1674-1056/21/12/124702

A combined airfoil with secondary feather inspired by the golden eagle and its influences on the aerodynamics

Di Tang(唐迪)[1,2,†], Zhongyong Fan(范忠勇)[3], Mingxia Lei(雷鸣霞)[3], Binbin Lv(吕彬彬)[2], Li Yu(余立)[2], and Hao Cui(崔浩)[4]

[1] *College of Mechanical Engineering, Zhejiang University of Technology, Hangzhou* 310014, *China*
[2] *High Speed Aerodynamic Institute, China Aerodynamics Research and Development Center, Mianyang* 621000, *China*
[3] *Zhejiang Museum of Natural History, Hangzhou* 310014, *China*
[4] *Shenyang Aircraft Design and Research Institute of AVIC, Shenyang* 110035, *China*

(Received 8 August 2018; revised manuscript received 17 December 2018; published online 25 February 2019)

Bird flight is a remarkable adaption that has allowed thousands of species to colonize all terrestrial habitats. A golden eagle has impressive flying abilities, such as hovering, perching, preying and attacking. To reveal the flying abilities, avian geometry of a golden eagle was extracted based on noncontact surface measurements using a ROMBER three-dimensional laser scanner. Distributions of a camber line, thickness and a secondary feather line of the extracted point cloud were fitted using convenient analytical expressions. A traditional airfoil was established with the camber line and thickness, then a combined airfoil was constructed by combining the traditional airfoil with a secondary feather. Oscillations of an airfoil as well as rapid pitch up were simplified as a sine wave around the quarter chord axis. Thereafter, both steady and unsteady aerodynamic performances of the airfoil are computed, the influences of the secondary feather on the steady and unsteady aerodynamics were further studied.

Keywords: aerodynamics, large prey, secondary feather, three-dimensional scanning

PACS: 47.32.cd, 47.32.Ff **DOI:** 10.1088/1674-1056/28/3/034702

1. Introduction

The ideal of flying origins from avian flying, and a lot of typical airplanes have been designed until now, such as B747, A320, F22, Su27, and so on. However, these traditional rigid airplanes were designed according to a particular flight envelope or some destined conditions, which will lead to fuel consumption, less manoeuvrability, and so on.[1] For instance, a low aspect ratio airplane flies faster with excellent manoeuvrability, but lack fuel efficiency. On the other hand, a high aspect ratio airplane flies slower, but with good aerodynamics and great fuel economy. With continuous requirements of excellent flight performance and control authority, the morphing wing concept has been proposed to provide improved aerodynamic properties over a great range of operating conditions, and a variety of types of wing morphing mechanisms have been proposed in either a passive way or an active way.[2] In general, three categories of morphing designs were reviewed by Zheng *et al.* in the view of shape generation:[3] (i) rotating a whole wing or only a selected segment, (ii) telescopic, (iii) inflating a whole wing or only a selected segment. Morphing of rotating, achieved by rotation of either parts or a whole wing, can be categorized as out of plane morphing wing, in plane morphing wing and morphing cellular truss structure with tendons. Morphing of telescopic is accomplished by extending or contracting a wing with some segments associated with progressively smaller cross-sections. Morphing of inflating is achieved by a packed volume more than 10 times smaller than the deployed one. Unlike the conventional approach to change shape of a wing by mechanisms such as hinged flaps, some smart materials have been proposed and used in current airplane designs especially in unmanned aerial vehicle designs (UAV).[4] The ideal material for a morphing structure is an integration of load-carrying, deformability and low weight as discussed by Xavier *et al.*[5] Until now, there have been several categories of materials concluded for morphing materials, and elastomer is a class of polymer having ability to undergo large strains with easy deforming talents because of its low stiffness. Anisotropic materials are also used for morphing designs for their stiffness are direction dependent which enable a structure to morph in a particular direction while stiff in others. Multistable materials, capable of holding several stable positions and have presented large deformation abilities, as well as some smart materials, such as auxetic materials, are also interesting morphing materials, more details about morphing can be found in Ref. [6].

Above all, morphing structures or morphing materials have been used in conventional airfoils, and lots of aircrafts have been designed with morphing abilities. However, none of the aircrafts ever designed has the perfect manoeuvrability like birds. Flying abilities of birds, such as hovering, soaring and perching are quite impressive. After thousands of years of evolution, a bird wing moves generally with complex patterns in both wing kinematics and deformations,[7]

†Corresponding author. E-mail: tangdi@zjut.edu.cn

© 2019 Chinese Physical Society and IOP Publishing Ltd

and a bird can colonize almost all terrestrial habitats on earth, such as polar region, distant islands, cliff, and many others. For this reason, researchers now returning their interests of birds' flight abilities. For instance, Stefano Buoso investigated on the bat-inspired integrally actuated membrane wings,[8] Hightower *et al.* investigated on the closed-loop performance of a two dimensional actuated membrane wing with fixed supports,[9] Ren *et al.* revealed the sound suppression mechanisms of eagle owls.[10] Different species of birds have different flight talents, more stories about bird flying can be found in references.[11–16] Avian wing geometries of large birds, such as seagull, merganser, teal and owl have been investigated,[17,18] geometry shape of a bird wing, including airfoils, can be quantified with analytical expressions, and a jointed arm model was also developed to represent the avian wing kinematics recovered from videos. Secondary feathers have important effects on bird aerodynamics, cutting of secondary feathers at wing tip was reported to reduce the distance flown dramatically.[19] It is impressive that the perching of steppe eagle Aquila nipalensis was studied[20] using onboard and high-speed video, wing shapes were recovered and unsteady aerodynamics were studied including role of aeroelastic feather deflection. It was figured out that one of the secrets in bird flying manoeuvrability is the ability of wing morphing that allows quick transition between a steady glide and a deep stall.

Above all, a key to excellent flight abilities of birds is that they can change their wing shapes in an intelligent and efficient way using their exclusive airfoils.[21] Until now, much efforts have been focused on wings with conventional airfoils. However, a secondary feather has played an important role in bird flight. Thus, a particular combined airfoil with a secondary feather and influences of a secondary feather on the aerodynamics during maneuvering are the main topic of this paper.

2. Specimen and experiment

2.1. Specimen of golden eagle

A golden eagle has quite excellent flying abilities to perch, fight, and so on. However, a golden eagle is one of the first-class national protected animals of China, any sale, purchase or use of the wild animal is forbidden. Thus, we corporate with Pro. Fan of Zhejiang Museum of Natural history. The scanning object is a specimen of golden eagle of Zhejiang Museum of Natural history as shown in Fig. 1. The golden eagle was processed at a flying posture and the specimen has been well kept. Before scanning, a kind of alcohol for a specimen was used to clear each feather. Also, each feather was repaired and rearranged to ensure the exact flying shape.



Fig. 1. Specimen of the golden eagle of Zhejiang Museum of Natural history

2.2. 3D scanning of a wing

We used a ROMBER absolute arm with integrated scanner to which a three-dimensional non-contact laser scanner was attached for the bird surface measurements. The ROMBER absolute arm is a hand-held mechanical device with high accuracy. Before measuring, the ROMBER tower was fixed to the ground using glue. On the ROMBER arm, position of the scanner relative to a given coordinate system is known accurately. An integrated laser scanner is designed to capture 3D point data across a range of surface types. With an ultra-wide laser stripe of up to 150 mm, the scanner can capture 7520,000 points per second. Accuracy of the complete scanning system is verifiable and traceable, accuracy of surface data is within 0.01 mm. Operating with Geomagic Wrap software, the system works based on the principle of laser stripe triangulation. During measurements, a laser line was project onto the wing feathers and the line was viewed by cameras so

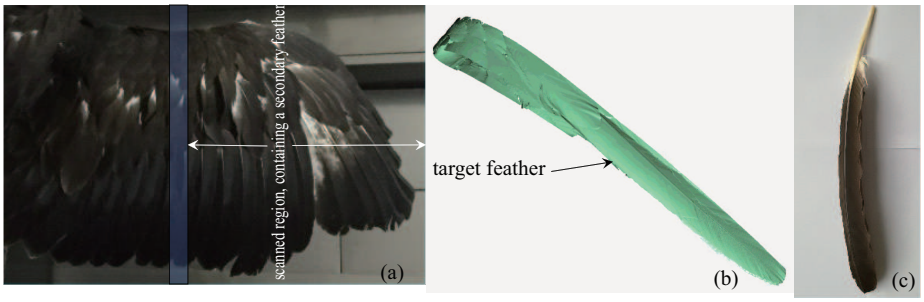


Fig. 2. The airfoil with a secondary feather: (a) the scanned region, containing a secondary feather; (b) the scanned point cloud; (c) the contained secondary feather.

that distance variations on a feather can be seen. In order to obtain a combined airfoil with excellent aerodynamic performances, the scanned region was limited at the middle of the span where a secondary feather existed, as shown in Fig. 2(a). Scanning data was a profile that contained airfoil information. The scanner can work for a variety of materials and colors including black and white which are common for feathers of a golden eagle. Figure 2(b) and 2(c) also show the scanned point cloud and the corresponding secondary feather. It can be expected that a 3D wing model can be established by assembling the combined airfoils at different stations.

3. Modeling and numerical method

3.1. Airfoil modeling

The combined airfoil is composed of a typical wing airfoil and a secondary feather airfoil, named as Part1 and Part2 respectively, as shown in Fig. 3. The main motivation for this classification is that the secondary feather may move or rotate relative to the part1, also some empirical functions have been figured out for capturing the typical airfoil of part1.

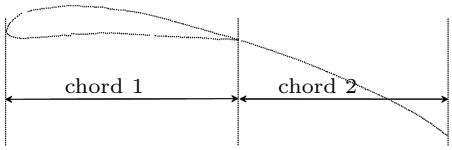


Fig. 3. Part1 and part2 of the combined airfoil with a secondary feather

As the part1, distributions of a camber line and thickness were quantified at first, thus the upper surface was expressed as an addition of the camber line and thickness, the lower surface was expressed as a subtraction of the camber line and thickness.

$$z_{\text{upper}} = z_{(\text{c})} + z_{(\text{t})}, \tag{1}$$

$$z_{\text{lower}} = z_{(\text{c})} - z_{(\text{t})}. \tag{2}$$

To quantify the mean camber line from wing surface measurements, the Birnbaum–Glauert camber line was used[22]

$$\frac{z_{(\text{c})}}{c} = \frac{z_{(\text{c})\max}}{c}\eta(1-\eta)\sum_{n=1}^{3} S_n(2\eta-1)^{n-1}, \tag{3}$$

where $\eta = x/c$ is the normalized chordwise coordinate, $z_{(\text{c})\max}$ is the maximum camber coordinate, c is the local wing chord length, coefficients S_n are to be determined. The thickness distribution was quantified as

$$\frac{z_{(\text{t})}}{c} = \frac{z_{(\text{t})\max}}{c}\sum_{n=1}^{5} A_n(\eta^{n+1} - \sqrt{\eta}), \tag{4}$$

where $z_{(\text{t})\max}$ is the maximum thickness, coefficients A_n are to be determined and order 6 was used here.

As the Part2, a local coordinate was arranged at the feather root, an exponential function was used to describe the bending of the secondary feather along the x axis

$$\frac{\omega_{(\text{t})}}{c} = \frac{\omega_{(\text{t})\max}}{c}\varphi\, \text{e}^{\psi}, \tag{5}$$

where $w_{(\text{t})\max}$ is the maximum bending at the tip of the secondary feather.

3.2. CFD method

Aerodynamic forces acting on flies or birds can be computed using the CFD method.[23] The governing equations are impressible Navier–Stokes equations which are solved using Fluent (of Fluent Inc., USA). SIMPLEC algorithm was used for pressure and velocity coupling. Pressure based solver was chosen with an explicit formulation. Space discretization scheme of pressure equation used second order, discretization scheme of momentum used Quick scheme. To get accurate solution, a small time step of 3×10^{-5} was used, which was estimate by the characteristic of oscillating vortexes. The continuity equations are

$$\frac{\partial u_i u}{\partial x_i} = 0. \tag{6}$$

The momentum equations are

$$\rho\left[\frac{\partial u_i}{\partial t} + \frac{\partial u_i u_j}{\partial x_j}\right] = \frac{\partial}{x_j}\left[\mu\frac{\partial u_i}{\partial x_j}\right] - \frac{\partial p}{\partial x_i}, \tag{7}$$

where t is the time, u is the velocity, p is the pressure, μ is the coefficient of dynamic viscosity.

Flow before an airfoil is usually laminar, while flow around an airfoil is mainly turbulent. The transition SST model which is more accurate and adaptive for such situation has been applied to the flapping wings.[24,25] Thus, the γ–θ transition model was used here to predict aerodynamics of the combined airfoil, further details of the SST model can be found in ANSYS manual. The transport equation[26–28] of γ and $\widetilde{\text{Re}_{\theta t}}$ are

$$\begin{aligned}&\frac{\partial(\rho\gamma)}{\partial t} + \frac{\partial(\rho U_i\gamma)}{\partial x_j}\\ &= P_{\gamma1} - E_{\gamma1} + P_{\gamma2} - E_{\gamma2} + \frac{\partial}{\partial x_j}\left[(\mu + \frac{\mu_t}{\sigma_\gamma})\frac{\partial\gamma}{\partial x_j}\right],\end{aligned} \tag{8}$$

$$\begin{aligned}&\frac{\partial}{\partial t}(\rho\widetilde{\text{Re}_{\theta t}}) + \frac{\partial(\rho U_j\widetilde{\text{Re}_{\theta t}})}{\partial x_j}\\ &= P_\theta + \frac{\partial}{\partial x_j}\left[\sigma_{\theta t}(\mu+\mu_t)\frac{\partial\widetilde{\text{Re}_{\theta t}}}{\partial x_j}\right].\end{aligned} \tag{9}$$

Aerodynamic performances of an airfoil are characterized by cycle lift coefficient (C_L) and drag coefficient (C_D). Both the lift coefficient and the drag coefficient are normalized with the upstream undisturbed flow velocity V, airfoil chord length C, air density ρ, and lift force L and drag force D.

$$C_\text{L} = \frac{L}{\frac{1}{2}\rho V^2 C}, \tag{10}$$

$$C_{\mathrm{D}} = \frac{D}{\frac{1}{2}\rho V^2 C}. \tag{11}$$

Vorticity in z direction is defined as follows:

$$\omega_z = \frac{\partial V_y}{\partial x} - \frac{\partial V_x}{\partial y}. \tag{12}$$

3.3. Numerical example of phase VI and S809 airfoil

The S809 airfoil model with a 457 mm constant chord was designed by OSU/AARL personnel, the airfoil was tested in the 3×5 subsonic wind tunnel under steady state and unsteady conditions at Ohio State University Aeronautical and Astronautical Research Laboratory.[29] The baseline conditions for steady was tested, angles of attack ranged from $-20°$ to $40°$. The unsteady behavior was examined by oscillating the airfoil about its pitch axis where three mean angles, three frequencies and two amplitudes were tested.

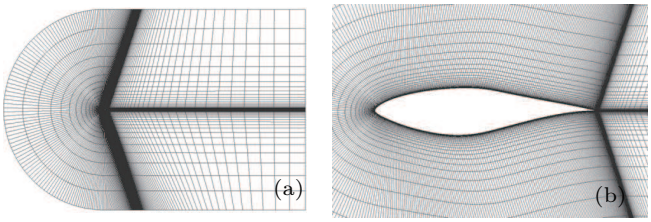


Fig. 4. Mesh of the S809 airfoil: (a) computational domain; (b) local view of the S809 airfoil.

To verify the computational method of this paper, figure 5 shows a comparison of the experimental data and computational results. The maximum positive lift coefficient and drag coefficient for the clean cases are about 1.06 and 0.77, respectively. The average lift curve slope is about 0.12. It is shown that the lift of S809 has a double stall. The stall first appears at 11.2°, then, the CL begins to increase until 15.2°, which were predicted exactly in this paper. A minimum of 0.67 of CL appears at 20°. It is shown that results of this paper fit well with the experimental data before 16.2°. However, there are deviations after 20° which is under deep stall.

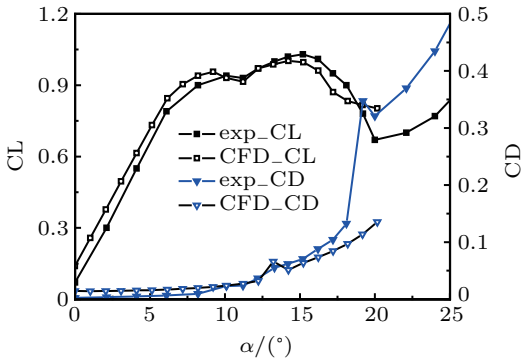


Fig. 5. CL and CD versus α of airfoil S809.

4. Results and discussion

Equations (3)–(5) are defined as user defined functions in the MATLAB software, then a curving fitting method is used to extract the coefficients S_n, A_n, φ, ψ for the camber line, thickness, and secondary feather from measurements of the golden eagle specimen as listed in Table 1. Thereafter, the interpolated normalized camber line, thickness and secondary feather are generated with those coefficients, as shown in Fig. 6(a). It is indicated that the measured data presents a statistical property pointed by Riegels,[22] and the fitted curves match with the measured data well. Figure 6(b) shows deviations of the fitting airfoil from the measurement points in terms of the local maximum values $z_{(\mathrm{c})\max}$, $z_{(\mathrm{t})\max}$ and $w_{(\mathrm{t})\max}$. Deviations of the camber line vary from -3.62% to 5.06%, deviations of the thickness distribution vary from -4.83% to 3.75%, deviations of the secondary feather vary from -5.26% to 4.68%. Above all, the maximum deviation is under 5.26% of all the three curve fittings.

Table 1. Coefficients determined for the camber line, thickness, and secondary feather of the combined airfoil.

S_1	S_2	S_3	A_1	A_2	A_3	A_4	A_5	φ	ψ
3.6	1.5	0.3	–4.8	66.2	–199.8	235.6	–97.6	0.003	5.7

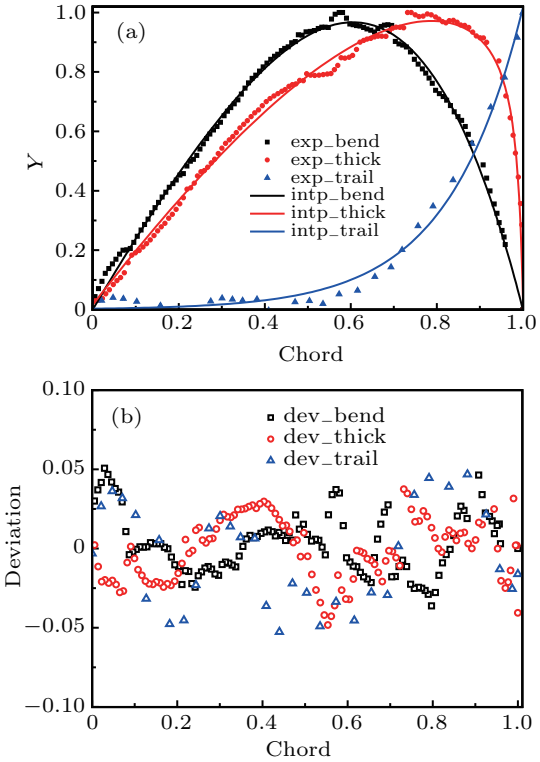


Fig. 6. Fitting airfoil: (a) camber line, thickness distribution, and tail line of the golden eagle; (b) deviation of local profiles from scanned profile.

An airfoil without any secondary feather was constructed with distributions of camber line and thickness using Eqs. (1) and (2), which is similar to the seagull airfoil or S1223 airfoil described by Liu.[17] Thereafter, a secondary feather was

installed to the airfoil without any secondary feather to construct the combined airfoil according to the rule of curvature continuity at upper surface. Figure 7 shows a comparison of the traditional airfoil and the combined airfoil. It should be mentioned that birds' feathers are flexible, which has insignificant influences on the aerodynamic performances. However, the original intention of this paper was to proposed a bird-inspired combined airfoil manufactured with rigid metal, composite materials, and so on. Thus, the elasticity of secondary feather and the corresponding aeroelasticity were not discussed. More information about the feather elasticity can be found in Ref. [30]

Then, an O-block technique was used to construct the mesh of the two airfoils, the close-up view of the meshes near the two airfoils are shown in Fig. 8. The traditional airfoil as well as Part1 of the combined airfoil were discretized with 403 nodes, while the secondary feather was discretized with 200 nodes. The radial size of the first layer was set according to the rule of non-dimensional wall distance y^+ less than 1, and the total elements of the two airfoils are about 42300 and 63200, respectively.

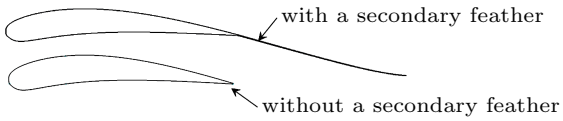


Fig. 7. A combined airfoil with a secondary feather and a traditional airfoil without a secondary feather inspired from the golden eagle.

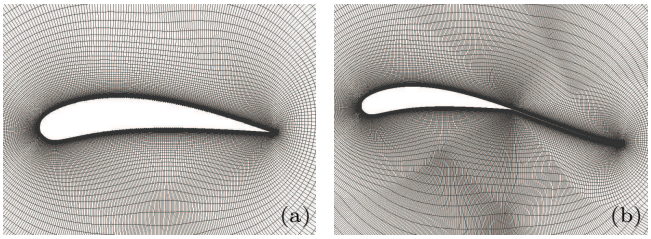


Fig. 8. Meshes of the two bionic airfoils: (a) the traditional airfoil; (b) the combined airfoil.

Kinematics of a flapping wing can be considered as a superposition of motions of the quarter chord axis and relative rotations around the axis. For simplicity, a sine wave form is defined by Eq. (13) to represent the relative rotation, and oscillating amplitudes with $\pm 30°$, $\pm 60°$, and $\pm 90°$ were used for the influence study

$$\alpha = \alpha_{\mathrm{m}} + A\sin(2\pi f t), \tag{13}$$

where α_{m} is the mean angle of attack, and A is the oscillating amplitude. The oscillating frequency is set according to wing motions. Rapid pitch-up is essential to the high manoeuvrability of a golden eagle during perching, flighting, and so on. Thus, a control strategy of airfoil rotation is designed here to study the unsteady aerodynamics using a sine wave

$$\alpha = \alpha_0 + \frac{A_{\mathrm{p}}}{2}\sin\left(\frac{2\pi}{2T}t - \frac{\pi}{2}\right) + \frac{A_{\mathrm{p}}}{2}, \tag{14}$$

where α_0 is the initial angle of attack, A_{p} is the respective amplitude, and T is the pitch up time.

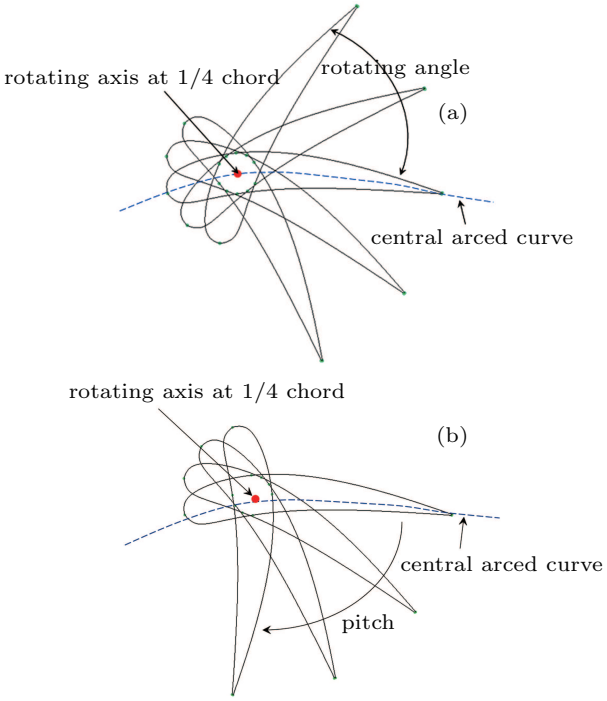


Fig. 9. Illustrations of motions of an airfoil: (a) sinusoidal oscillation controlled by Eq. (13); (b) rapid pitch controlled by Eq. (14).

4.1. Influences on the static aerodynamic performances

Drags and lifts of the traditional airfoil, named as WITHOUT case, were computed over a nominal angle from $-10°$ to $30°$, while similar forces were computed for the combined airfoil, named as WITH case, as shown in Fig. 10. The maximum lift and the maximum drag are 22.8 N and 3.3 N, respectively for the WITHOUT case, while 39.2 N and 10.1 N for the WITH case, a 71.9% increase and a 206.1% increase, respectively. It is indicated that a secondary feather has great effects on consistently lift enhancement and drag enhancement through a wide range of angles of attack.

Furthermore, non-dimensional lift coefficient CL and drag coefficient CD were compared to ignore the scale effect raised by the secondary feather as shown in Fig. 11. As the CL, a maximum value 1.97 appears at $\alpha = 8°$ of the WITH case and the lift coefficient begins to decrease monotonically as angle of attack increases beyond $8°$, on the contrary, the lift coefficient achieves a maximum value 1.98 at $\alpha = 16°$ of the WITHOUT case and decreases monotonically as α beyond $16°$. It is interesting to find that the maximum values of CL of the two cases coincide with each other with only a 0.6% fluctuation. As the CD, drag coefficients increase against angle of

attack in a wide range from −5° to 30° of the two cases. In consideration of the similarities, coefficients of lift and drag of the WITH case were transferred by +6° depicted with green color in Fig. 11. It is found that both the CL and the CD of the WITH case are consistent with those of the WITHOUT case when α is under 15°. However, as α keeps increasing, the CL of the WITH case deviates from the WITHOUT one by 0.27.

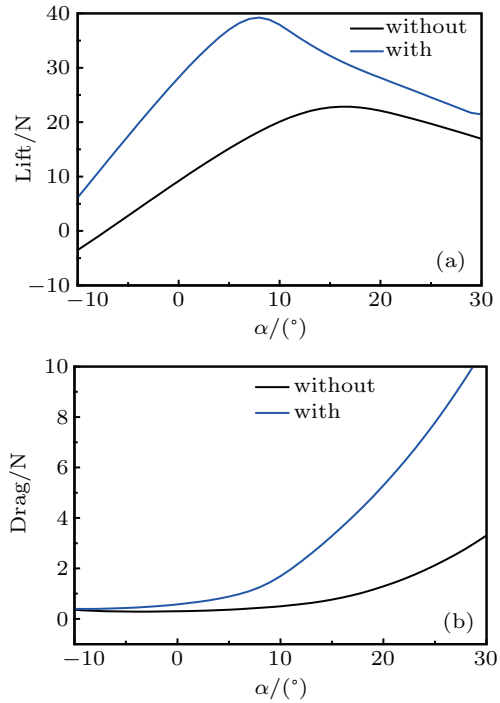


Fig. 10. Lifts and drags of the two airfoils: (a) lift; (b) drag.

Two similar maximum lift coefficients were found for both the WITHNOT case and the WITH case, to figure out the corresponding flow characteristics, pressure distributions and streamlines were illustrated in Fig. 12. At $\alpha = 8°$, a small separation appears at the trailing edge of the secondary feather in the WITH case while no separation was found in the WITHNOT case. To obtain the maximum CL of 1.98, the traditional airfoil should suffer a larger angle of attack of 16°. In contrast to the WITHNOT case at $\alpha = 16°$, the minimum pressure coefficient has been drastically decreased from −5.2 to −6.4. Meanwhile, the existing area of the pressure coefficient range from 08 to 1.0 has been enlarged from the leading to the Part2 of the combined airfoil. The effect of the secondary feather is not to enlarge the maximum pressure coefficient which is a theoretical value of 1.0, but to enlarge the existing area with high pressure.

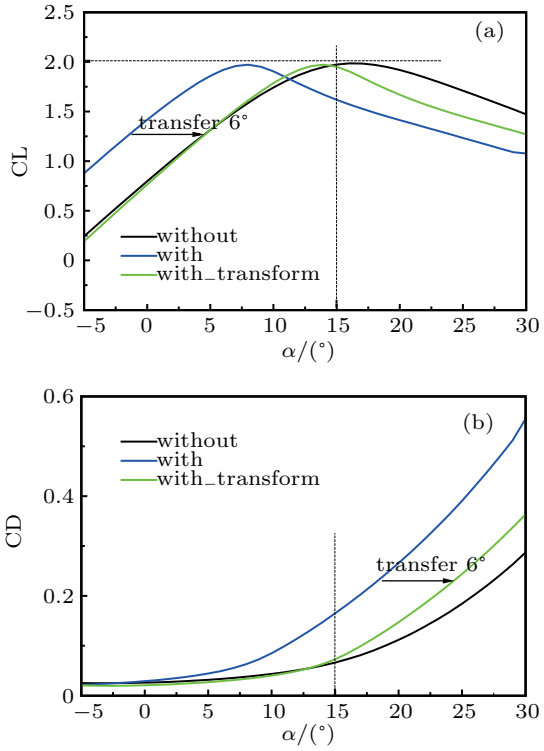


Fig. 11. CL and CD of the two airfoils: (a) CL; (b) CD.

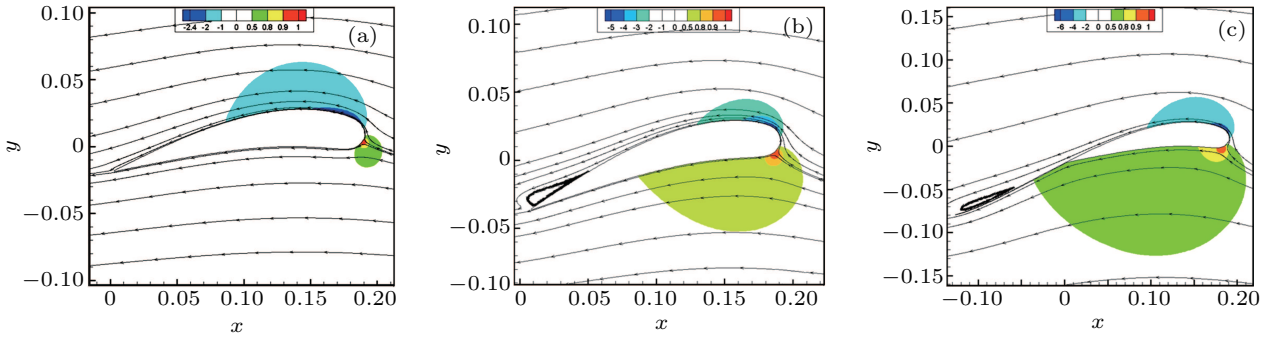


Fig. 12. Pressure coefficient and streamline distributions: (a) WITHNOT case at $\alpha = 8°$; (b) WITHNOT case at $\alpha = 16°$; (c) WITH case at $\alpha = 8°$.

4.2. Influences on the dynamic aerodynamic performances

To obtain effects of the secondary feather on the unsteady aerodynamics, unsteady numerical data was obtained for both the WITHNOT case and the WITH case undergoing sinusoidal oscillations. A comprehensive set of conditions were tested to demonstrate unsteady behaviors at oscillating frequency of 3.125 Hz, with oscillating amplitude A equal to 30°, 60°, and 90°, respectively. Figures 13(a) and 13(b) show CL versus α

to represent the effect of oscillating amplitude. The pre-stall lift coefficient achieves a maximum value of 4.3 during the upstroke and a minimum value of −3.6 during the down stroke at $A = 90°$ of the WITHNOT case, as suggested that airfoils always suffer a higher CL during an upstroke. The stall recovery is delayed leading to an appearance of hysteresis loop, which were exhibited throughout all of the oscillating cases. Furthermore, both the maximum CL and width of a hysteresis loop increase as the oscillating amplitude increasing. Similarly, drag coefficients versus the angle of attack were also shown in Figs. 13(c) and 13(d), the maximum drag and the width of hysteresis loop obtain a maximum value at a higher oscillation amplitude.[31]

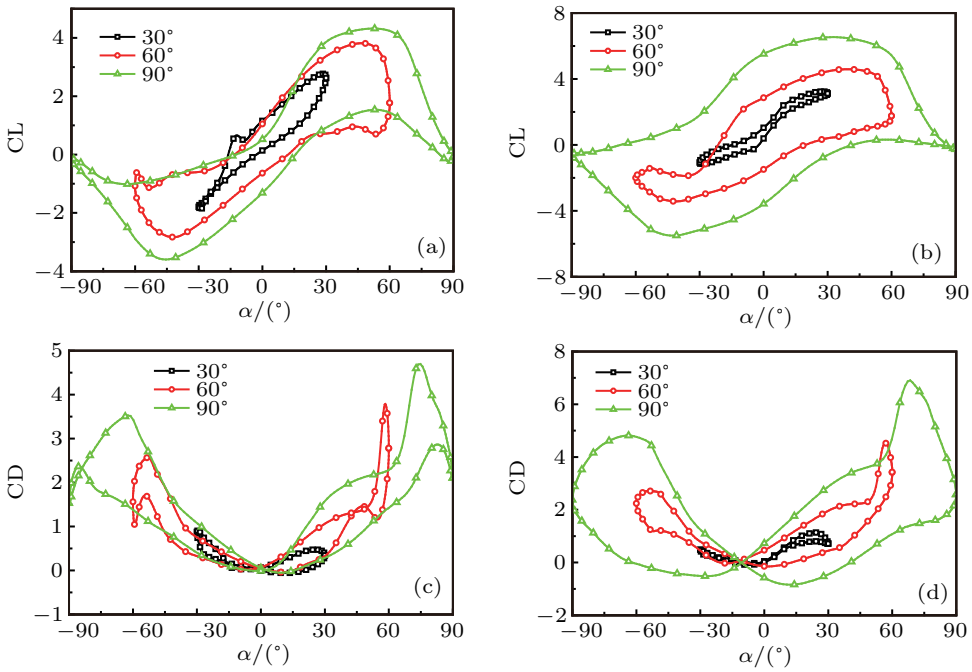


Fig. 13. Lift and drag coefficients of the two oscillating airfoils at frequency of 3.125 Hz: (a), (b) lift coefficients for WITHNOT and WITH cases, respectively; (c), (d) drag coefficients for WITHNOT and WITH cases, respectively.

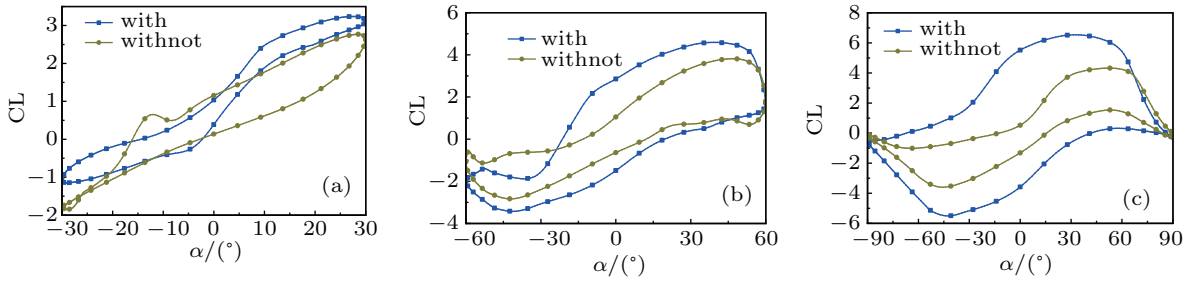


Fig. 14. Comparison of CL for the WITH and WITHNOT cases: (a) $A = 30°$; (b) $A = 60°$; (c) $A = 90°$.

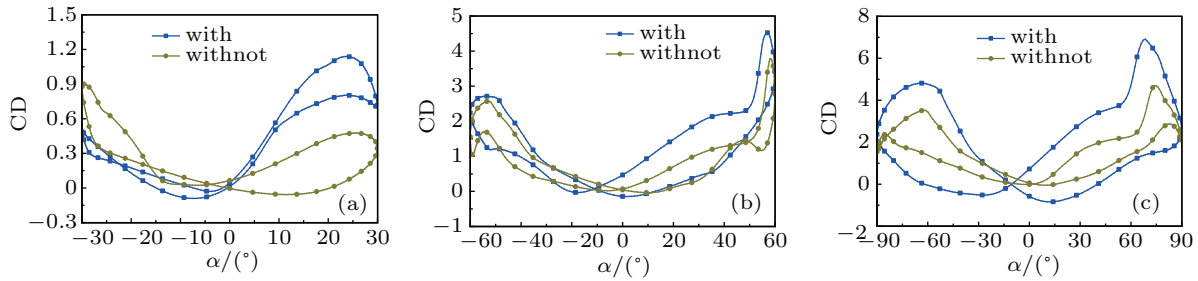


Fig. 15. Comparison of CD for the WITH and WITHNOT cases: (a) $A = 30°$; (b) $A = 60°$; (c) $A = 90°$.

CL and CD for both the WITH case and the WITHNOT case were also compared in Fig. 14 and Fig. 15. The CL achieves a maximum value of 3.23 for the WITH case at $A = 30°$, increased by 17% compared with the one of 2.76 of the WITHNOT case. Similarly, the CL achieves a maximum value of 4.59 at $A = 60°$ and a maximum value of 6.54 at $A = 90°$ for the WITH case, the corresponding increments are 20% and 51%, respectively. In comparison, the maximum

drag coefficient is 1.1, 4.52, and 6.91 for the WITH case at $A = 30°$, $60°$, and $90°$, respectively, increased by 22%, 21%, and 50% compared with the maximum value of 0.9, 3.78, and 4.69 of the WITHNOT cases. It is indicated that effects of the secondary feather on the maximum CL and CD are more pronounced by the oscillating amplitude. These differences between WITHNOT and WITH cases are the main reason that a secondary feather should be required for the aerodynamic analysis of a bird.

4.3. Aerodynamics of pitch up

It should be noted that the conventional design or optimization objective is usually a high lift-drag ratio. However, the key to high manoeuvrability in bird flight lies not in the high lift-drag ratio, but in the way that a wing morph to adjust flying situations. Take the flight of a steppe eagle for example which was investigated by Carruthers, before perching, the Steppe Eagle "Aquila nipalensis" flied with wings held fixed in an outstretched posture followed with a rapid pitch-up when approaching its perch. Here, we studied fighting of two eagles.[32] It is shown that Eagle A dived towards Eagle B with an attack appearance at 0.0 s. Then, Eagle A pitched up the wing within about 0.08 s aimed at changing attitude of diving to deep stall. During the fighting no flapping was observed of the wing but rapid pitch up. During the rapid pitch-up, kinetic energy of the eagle was exchanged to gravitational potential energy. Previously on the comparison of CL illustrated in Fig. 14, the CL can be enlarged incredibly at angles of attack ranging from 0° to 90° during a up stroke, which will drive a bird upward. Finally, a deep stall appears after the end of pitch up followed by incredible increase of drag, thus the total kinetic energy is dissipated into the air.

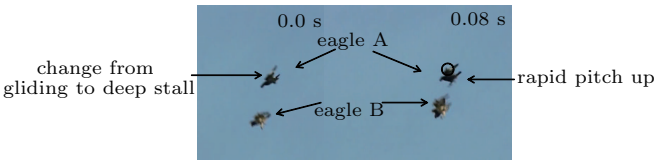


Fig. 16. Fight between Eagle A and Eagle B, dive was adopted followed with a Rapid pith up by Eagle A to slow down within 0.08 s.[32]

To investigate the corresponding aerodynamics, control strategy of angle of attack is defined using Eq. (13), and here parameters are set as $\alpha_0 = 0°$, $T = 0.08$, $A_p = \pi/2$ in order to ensure that the combined airfoil will pitched up to $\pi/2$ from 0° within 0.08 s. The CL and CD against α were demonstrated in Fig. 17 with similar tendencies illustrated in Figs. 13(b) and 13(d). It is shown that the CL achieves a maximum value of 6.97 at $\alpha = 40.0°$, which is 6% greater than 6.54 of the corresponding oscillating case, and the CD reaches a maximum value of 7.05 at $\alpha = 61.875°$. Above all, it is interesting to find that the maximum drag coefficient appears at 61.875° instead of 90° with dramatical increase of 137.4% against the 2.97 at $\alpha = 90°$. It is expected that both the high CL and the high CD executed by the rapid pitch up offer an opportunity to change the flight attitude quickly. Thus, the research of this paper can be a good suggestion for the unmanned aerial vehicle design of the next generation.[34,35]

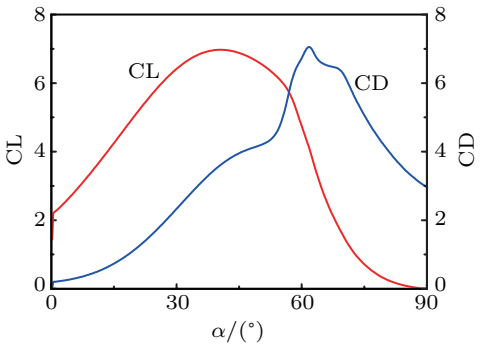


Fig. 17. CL and CD of the combined airfoil with a secondary feather during rapid pitch up.

To reveal the generating mechanism of fantastic high CD and CD during rapid pitch up, a sketch of vortexes superimposed on the instantaneous streamlines around the combined airfoil was depicted in Figs. 18(a)–18(d) between 0 s and 0.08 s. At the initial station, $\alpha = 0°$, air keeps attached at both the leading edge and the trailing edge. As angle of attack increases to 39.375° where a maximum lift coefficient is obtained, a stronger leading-edge vortex is generated to cover the upper surface, meanwhile air begins to separate from the trailing edge.[33] When α increases to 61.875° where a maximum drag coefficient is obtained, the generated vorticity begins to separate and dissipate from the upper surface. Air rolls up tightly from the leading edge with anti-clockwise rotation, meanwhile, rolls downstream with a strong intensity to induce a second leading edge vortex. This roll-up and roll downstream continue as the airfoil pitch up, and the second leading edge vortex rolls up forward on the airfoil's surface gradually. As α continues to 90°, the separated vortex moves away from the upper surface.

Pressure distributions between 0 s and 0.08 s were also investigated to examine the high drag coefficient, as shown in Figs. 19(a)–19(d). As the combined airfoil is pitched up to 61.875°, a region with low pressure extends downstream from the upper surface to induce a deep attractive force in the drag direction, which is consistent with the vortex distribution depicted in Fig. 18(c). A region with high pressure also distributes in succession from the secondary feather to the trailing edge, which causes a large thrust in the drag direction. Combined the attractive force with the thrust, a maximum drag force is formed. Benefitting from large length of the secondary feather, pressure near the down surface of the secondary feather is increased significantly. Therefore, the maximum drag coefficient appears at 61.875° rather than 90°.

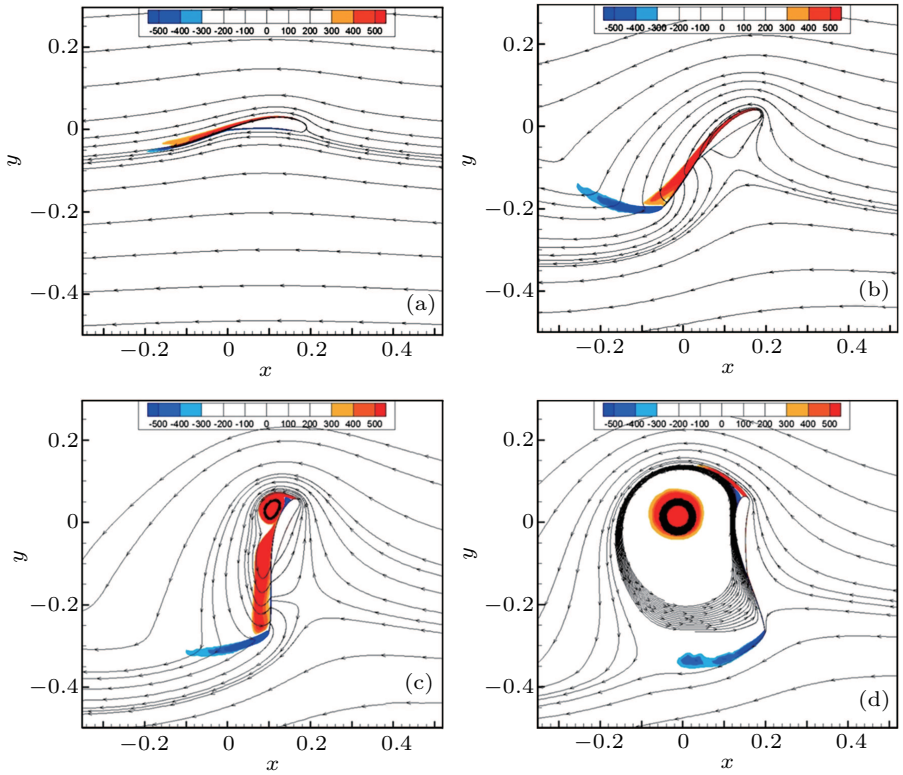


Fig. 18. Vortexes and stream lines of the airfoil with a secondary feather during rapid pitch up: (a) $t = 0.0$ s, $\alpha = 0°$; (b) $t = 0.035$ s, $\alpha = 39.375°$; (c) $t = 0.055$ s, $\alpha = 61.875°$; (c) $t = 0.080$ s, $\alpha = 90°$.

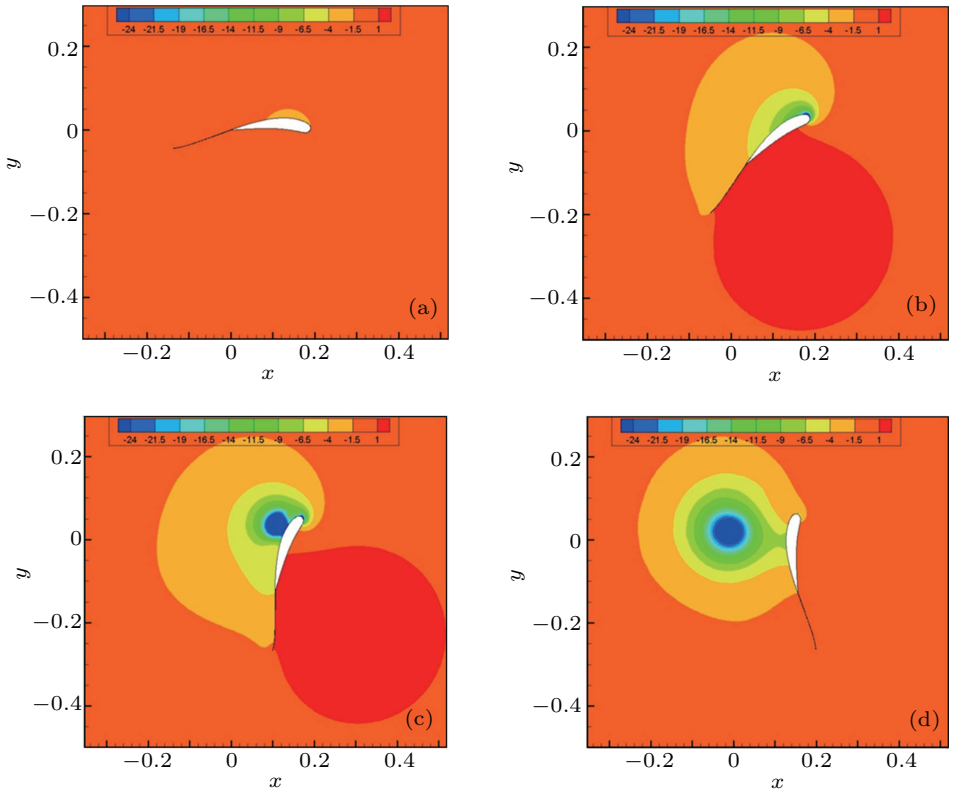


Fig. 19. Pressure coefficients of the combined airfoil during rapid pitch up: (a) $t = 0.0$ s, $\alpha = 0°$; (b) $t = 0.035$ s, $\alpha = 39.375°$; (c) $t = 0.055$ s, $\alpha = 61.875°$; (c) $t = 0.080$ s, $\alpha = 90°$.

5. Conclusion

In this study, the surface geometry of a golden eagle as well as a secondary feather were measured by a 3D laser scanner approach. From measurements, the airfoil camber line, airfoil thickness and the secondary feather camber line were extracted. The accuracy of the measurements using the laser scanner was 0.01 mm. Deviations of the fitting airfoil from

the measurement points were less than 5.26%. Thereafter, a traditional airfoil without a secondary feather and another combined one with the secondary feather were constructed. A CFD method with a deep insight about the suitability of numerical methods was verified to examine effects of the secondary feather on the unsteady aerodynamics. Then, both steady and unsteady aerodynamic performances have been studied.

For the steady case, influences of the secondary feather on the CL and CD were investigated. It is found that the maximum CL of the WITH case is almost the same with the WITHOUT case which are 1.97 and 1.98, respectively, the corresponding angle of attack are 8° and 16°, respectively. When the CL and the CD of the WITH case are transferred by 8°, it is interesting to find that both the CL curve and the CD curve fit well with the one of WITHOUT case under 15°, which indicates that the existence of the secondary feather does not change the steady aerodynamic coefficiences essentially but to enlarge the lift and drag by 71.9% increases and 206.1% in consideration to the large chord length.

Then, the unsteady performances were studied in which kinematics of an oscillating airfoil were simplified as translation of the quarter-chord line superposed with relative rotation around the quarter chord line. It has been found that the stall recovery is delayed and a hysteresis loop exhibits throughout all of the oscillating cases. The maximum lift and the maximum drag increase with the increment of the oscillating amplitude. The secondary feather has enlarged the maximum value of CL and CD during up stroke and decreased the minimum value of CL and CD during down stroke. Thus, a secondary feather should be required for aerodynamic analysis of a bird.

In fact, oscillating of a wing is rare in bird flight but rapid pitch up is the most common. Thus, unsteady performances were studied and the combined airfoil is simplified to pitch up rapidly with a control strategy of a sine wave form according to a bird flight. It is shown that lift coefficient achieves a maximum value of 6.97 at 39.375° and drag coefficient reaches a maximum value of 7.05 at 61.875°. During the pitch up, a stronger leading-edge vortex has been rolled up and downstream. It is interesting to find that the maximum drag coefficient appears at 61.875° instead of 90°.

Above all, both the secondary and the rapid pitch up play an important role in high manoeuvrability of a large prey, and a secondary feather has enabled a bird to fly with more excellent aerodynamics. It can be expected that the research of this paper can be a good suggestion for the unmanned aerial vehicle design of the next generation.

Acknowledgment

The authors would like to thank the team of Zhongyong Fan for all their contributions on the specimen and the 3D scanning.

References

[1] Ajaj R M, Friswell M I, Bourchak M and Harasani W 2016 *Aerosp. Sci. & Technol.* **53** 38
[2] Silvestro B, Onur B, Rafic A, Michael I F and Daniel I 2011 *J. Intell. Mater. Syst. & Struct.* **22** 823
[3] Zheng M, Vu Khac Kien and Richard J Y 2010 *IES J. Part. A: Civ. & Struct. Eng.* **3** 188
[4] Meng B Q, Han G L, Zhang D L and Jiang Z L 2017 *Chin. Phys. B* **26** 114702
[5] Xavier L, Stephen D and Weaver M 2013 *Wind Energy* **16** 283
[6] Stephen Daynes and Weaver M 2013 *Proc. Inst. Mech. Eng. Part. D J. Automobile Eng.* **227** 1603
[7] Thomas W and Robert K 2015 *Exp. Fluids* **56** 1
[8] Stefano Buoso, Dickinson T and Rafael Palacios 2017 *Bioinspiration & Biomimetics* **13** 016013
[9] Hightower J, Rivers I, Chin D, Carl L, Haselsteiner F and David L 2017 *Bioinspiration & Biomimetics* **12** 064001
[10] Chen K, Liu Q, Liao G, Yang Y, Ren L, Yang H and Chen X 2012 *J. Bionic Eng.* **9** 192
[11] Rao C, Ikeda T, Nakata T and Liu H 2017 *Bioinspiration & Biomimetics* **12** 046008
[12] Winzen A, Klaas M and Schröder W 2013 *Exp. Fluids* **54** 1472
[13] Moller A P and Swaddle J 1998 *Asymmetry, Developmental Stability, and Evolution* (Oxford: Oxford University Press)
[14] Ákos Z, Nagy M and Vicsek T 2008 *Proc. Natl. Acad. Sci. United States Am.* **105** 4139
[15] Warrick R, Tobalske W and Powers R 2009 *Proc.: Biol. Sci.* **276** 3747
[16] Liu X and Liu X 2014 *Adv. Mech. Eng.* **6** 859308
[17] Liu T S 2006 *AIAA. J.* **44** 954
[18] Ren H H, Wang X S, Chen Y L and Li X D 2012 *Chin. Phys. B* **21** 034501
[19] Brown E and Cogley C 1996 *J. Exp. Zool. Part. A Ecological Genet. & Physiol.* **276** 112
[20] Carruthers A C, Thomas A L R, Walker S M and Taylor G K 2010 *Aeronautical J.* **114** 673
[21] Videler J 2006 *Avian Flight* (Oxford: Oxford University Press)
[22] Riegels F W 1961 *Aerofoil Sections. Butterworths London Chaps.* **1** 7
[23] Zhou A, Xiu X Q, Zhang R, Xie Z L, Hua X M, Liu B, Han P, Gu S L, Shi Y and Zheng Y D 2013 *Chin. Phys. B* **22** 017801
[24] Zhao D M and Zhang Q C 2010 *Chin. Phys. B* **19** 030518
[25] Jiang S N, Li X, Ma L, Gao Y R, Gui W L and Cheng C F 2015 *Chin. Phys. Lett.* **32** 104209
[26] Tang D, Bao S, Xu M, Luo L, Lv B, Yu L and Cui H 2019 *Ann. Nucl. Energy* **124** 198
[27] Qing Y, Cao S Y and Liu S Y 2014 *Acta Phys. Sin.* **63** 214702 (in Chinese)
[28] Zhang X P and Zhao Q 2014 *Chin. Phys. B* **23** 064703
[29] Ramsay R R, Hoffman M J and Gregorek G M 1996 *Effects of Grit Roughness and Pitch Oscillations on the S809 Airfoil*. Nrel/TP-442
[30] Chen H, Rao F, Shang X, Zhang D and Hagiwara I 2013 *J. Bionic Eng.* **10** 341
[31] Mahboubidoust A, Ramiar A and Dardel M 2017 *Theor. & Appl. Mech. Lett.* **7** 185
[32] http://tv.cctv.com/ 2016/09/03/VIDEIE9btf74ldkkCHRmafEr160903.shtml
[33] Lu Y and Shen G X 2008 *J. Exp. Biol.* **211** 1221
[34] Joo J, Reich W and James T 2009 *J. Intell. Mater. Syst.* **20** 1969
[35] Murugan S, Saavedra Flores E I, Adhikari S and Friswell M I 2012 *Compos. Struct.* **94** 1626